GA–A23019



# DISRUPTION MITIGATION STUDIES IN DIII–D

by
P.L. TAYLOR, A.G. KELLMAN, T.E. EVANS, D.S. GRAY,
D.A. HUMPHREYS, A.W. HYATT, T.C. JERNIGAN, R.L. LEE,
J.A. LEUER, S.C. LUCKHARDT, P.B. PARKS,
M.J. SCHAFFER, D.G. WHYTE, J. ZHANG



JANUARY 1999

GENERAL ATOMICS

## DISCLAIMER

## DISCLAIMER

Portions of this document may be illegible in electronic image products. Images are produced from the best available original document.

GA–A23019

# DISRUPTION MITIGATION STUDIES IN DIII–D

by
P.L. TAYLOR, A.G. KELLMAN, T.E. EVANS, D.S. GRAY,*
D.A. HUMPHREYS, A.W. HYATT, T.C. JERNIGAN,† R.L. LEE,
J.A. LEUER, S.C. LUCKHARDT,* P.B. PARKS,
M.J. SCHAFFER, D.G. WHYTE,* J. ZHANG*

This is a preprint of an invited paper to be presented at the Fortieth Annual Meeting American Physical Society, Division of Plasma Physics, November 16–20, 1998, New Orleans, Louisiana and to be published in *Phys. Plasmas.*

*University of California, Los Angeles, California.
†Oak Ridge National Laboratory, Oak Ridge, Tennessee.

Work supported by
the U.S. Department of Energy
under Contract Nos. DE-AC03-99ER54463, DE-AC05-96OR22464,
DE-AC02-76CH03073, and Grant No. DE-FG03-95ER54294

GA PROJECT 30033
JANUARY 1999

## ABSTRACT

Data on the discharge behavior, thermal loads, halo currents, and runaway electrons have been obtained in disruptions on the DIII–D tokamak [J.L. Luxon and L.G. Davis, Fusion Technology **8**, 2A 441 (1985)]. These experiments have also evaluated techniques to mitigate the disruptions while minimizing runaway electron production. Experiments injecting cryogenic impurity "killer" pellets of neon and argon and massive amounts of helium gas have successfully reduced these disruption effects. The halo current generation, scaling, and mitigation are understood and are in good agreement with predictions of a semianalytic model. Results from "killer" pellet injection have been used to benchmark theoretical models of the pellet ablation and energy loss. Runaway electrons are often generated by the pellets and new runaway generation mechanisms, modifications of the standard Dreicer process, have been found to explain the runaways. Experiments with the massive helium gas puff have also effectively mitigated disruptions without the formation of runaway electrons that can occur with "killer" pellets.

# I. INTRODUCTION

During a tokamak disruption, the rapid and complete loss of the thermal and magnetic energy result in high thermal and electromagnetic loads on the vessel and internal components and sometimes generate intense high energy runaway electron beams.[1–4] Critical to the tokamak concept along with the operation of future devices, is the development of techniques to terminate the discharge safely and mitigate the destructive effects of disruptions. A disruption in the International Thermonuclear Experimental Reactor (ITER)[5] could result in the rapid loss of 1 GJ of energy leading to damage and reduced lifetime of the first wall of the vessel.[5] Research on the DIII–D[6] tokamak and elsewhere has shown that some of these disruption phenomena are highly nonaxisymmetric, giving rise to local thermal and electromagnetic loads that are much higher than the average.[1,7–14] In a series of dedicated disruption experiments described here, further data have been obtained on the thermal loads to the first wall, the structure and amplitude of the halo currents, and runaway electrons. Major disruptions and vertical displacement events (VDEs) have been investigated and techniques to mitigate the disruptions while minimizing runaway electron production have also been evaluated.

The results presented here extend the work previously reported.[7–10,15–16] The paper is organized as follows: the disruption phenomenology is discussed in Section II, the halo current data and modeling results are reported in Section III, the results of mitigation experiments on DIII–D are reported in Section IV, and the summary and conclusions are presented in Section V.

## II. DISRUPTION PHENOMENOLOGY

Disruption experiments on DIII–D were performed in deuterium discharges, typically lower single-null divertors with plasma current $I_p$ = 1–1.5 MA, toroidal field B = 1.8–2.1 T, major radius R = 1.7 m, minor radius 0.6 m, and elongation 1.2–1.8. Deuterium neutral beam heating was generally used.

Disruptions, including the experiments performed here, can generally be divided into one of two basic categories: major disruptions and VDEs that lead to a disruption. These two types differ in the sequence of disruption events. In a major disruption, the plasma first becomes unstable due to reaching an operational limit, such as a density limit or beta limit, that leads to the growth of a large magnetohydrodynamic (MHD) mode. The large MHD causes a loss of nested confinement surfaces. The thermal energy is rapidly lost (thermal quench) and the current profile flattens causing a drop in the plasma inductance and a corresponding spike up in the current. Finally, the high resistivity of the cold plasma results in a rapid decay of the plasma current (current quench). Frequently, as a consequence of the change in the current profile, the plasma energy, and the plasma radial position, the vertical position in a major disruption is lost after the thermal quench. In a VDE, the results are similar but the sequence is different. The first event is a loss of the vertical position, and the plasma moves vertically with the cross section and edge safety factor, q, decreasing as the plasma scrapes off against the first wall. The plasma then disrupts: the thermal quench occurs (typically, there is no current spike) followed by the current quench. Most of the experiments reported here were performed using VDEs because of the ability to reproducibly trigger the disruption to occur at a time where the diagnostics are optimized. Disruption effects evaluated include the current decay rate, the halo current, the halo current toroidal asymmetry, the power radiated, and the heat flux to the first wall. The two major effects investigated and mitigated in these experiments are the halo currents and the heat flux.

Halo currents are currents generated during the disruption that flow along open field lines surrounding the plasma, in what is known as the "halo" region, and return poloidally through the vessel.[1,9–10] Large forces on the vessel components can result when these poloidal halo currents interact with the toroidal field. Note that the toroidal halo currents do not contribute to forces on the vessel since they do not flow in the vessel wall. A number of experiments have also observed significant toroidal asymmetries[7,11–12] in the halo currents that can result in concentrated local forces larger than the average. The halo current measured on DIII–D for a typical triggered VDE [Fig. 1(b)] reaches ~20% of the predisruption plasma current.[7] The halo current is toroidally asymmetric and the degree of asymmetry is quantified in terms of the toroidal

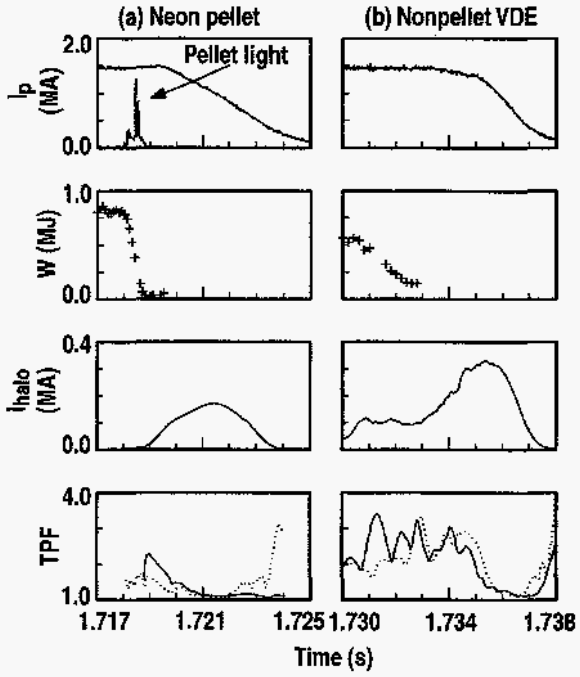


Fig. 1. Comparison of a VDE discharge mitigated with a neon pellet [(a) discharge 88826] versus an unmitigated VDE [(b) discharge 88810]. Time evolution of plasma current, pellet light, stored thermal energy calculated from equilibrium fitting code, the total poloidal halo current and TPF of the halo current measured by divertor floor toroidal arrays at major radius R = 1.08 m, 1.20 m (dotted).

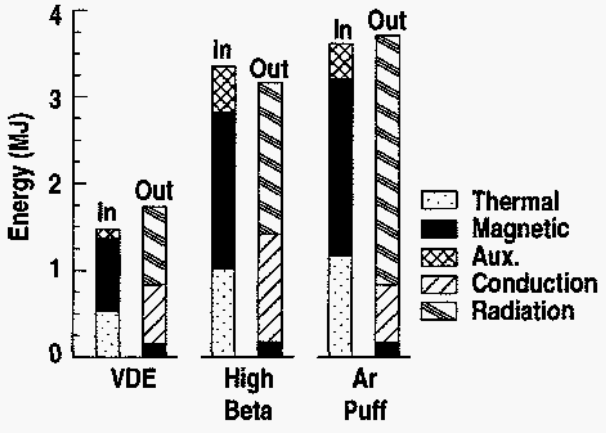


Fig. 2. Energy balance accounting of the energy input to the disruption (IN), which includes initial stored thermal energy, initial magnetic energy, and energy input during the disruption from auxiliary heating, versus the energy lost during the disruption (OUT) which includes radiation and conduction losses and the residual magnetic energy at the final analysis time. Results for three types of disruptions: VDE, high beta, and argon gas puff.

peaking factor (TPF) which is defined as the ratio of the peak of the toroidal current distribution to the toroidally averaged value. The time dependence of the TPF is also shown in Fig. 1 for two halo current monitoring arrays in the divertor floor at different major radii. Note that at the time of peak halo current, the TPF is reduced. Results from a number of DIII–D experiments show that at the time of peak halo current, TPFs approaching 3 are seen and halo currents range up to 35% of the initial plasma current.

The second disruption effect of interest is the heat flux. Detailed measurements of the heat flux to the divertor floor in DIII–D and the energy flow across a closed surface surrounding the plasma have been previously reported.[8,15–16] The stored thermal energy is lost during the thermal quench via radiation and conduction while the stored magnetic energy is lost during the current quench largely by radiation. For three disruptions, a VDE, a high beta disruption, and a disruption due to a large injection of argon gas an energy balance can account for the total energy loss during the disruption to within 15%. The energy input to the disruption (Fig. 2) includes the initial stored thermal energy and magnetic energy along with the energy added during the disruption by auxiliary neutral beam heating. The energy out includes the energy lost via radiation and conduction during the disruption and the residual magnetic energy at the final analysis time. Note that the initial energy stored in the magnetic field flows into the plasma during the current quench and is lost as radiation.

## III. DISRUPTION MODELING

The phenomenology of the axisymmetric component of the halo current, both its origin and evolution, is now well understood. The halo current time evolution in DIII–D disruptions have been accurately modeled with the DINA code,[17] a time-dependent, 1.5-dimensional (1.5-D), axisymmetric, resistive MHD and transport plasma simulation code. A simple analytic model, however, can be used to describe and explain the halo currents.[18] This model simulates the plasma and halo interaction via a simple circuit equation:

$$L_h \frac{dI_h^{tor}}{dt} + R_h I_h^{tor} = -M_{hp} \frac{dI_p^{core}}{dt} - \frac{1}{q_h} \frac{d\phi_h}{dt} \quad ,$$

where $I_h^{tor}$ is the toroidal halo current (current on open field lines); $I_p^{core}$ the core plasma current (current contained within the last closed flux surface); $\phi_h$ the toroidal flux linked by the halo current; $L_h$, $R_h$, and $q_h$ are the effective inductance, resistance, and safety factor of the halo region; and $M_{hp}$ the mutual inductance between the core and halo plasmas. The toroidal currents in the halo are induced by the decay of the toroidal core plasma current and by changes in the enclosed toroidal flux (i.e., changes in the plasma geometry). The model shows that the transfer of toroidal current from the core to the halo depends on the characteristics of the halo and core plasmas during the disruption. The toroidal halo current is approximately proportional to the ratio of the core current decay rate to the halo current decay rate which is, in turn, proportional to the ratio of the core-to-halo resistivities (lower temperature halos have lower halo currents). The model also shows that in VDEs, the vertical instability is a factor with the halo current proportional to the ratio of the vertical instability growth rate to the core current decay rate ($\gamma_z/\gamma_p$). While the current decay drives toroidal halo current, a poloidal current is also produced since in the halo region the plasma is force free ($\nabla p = J \times B \sim 0$) and the current flows along the open field lines. From the force-free constraint, a simple relation between the poloidal and toroidal halo currents can be derived showing they are proportional and related by the q of the field lines $\left(I_h^{pol} = I_h^{tor}/q\right)$.[18] An experimental scan of the vertical instability growth rate $\gamma_z$ was performed by varying the plasma beta and elongation. The poloidal halo current increases with $\gamma_z$ and the model predictions are in good agreement with both the experimental measurements of the peak halo current (Fig. 3) and with the time history measurement of the halo current in DIII–D VDEs.[8,18] The relation $\left(I_h^{pol} = I_h^{tor}/q\right)$ shows that high poloidal halo currents can arise when the edge q is low. To understand this evolution of the poloidal halo current, we examine VDE discharges in two regimes, $\gamma_z/\gamma_p < 1$ and $\gamma_z/\gamma_p > 1$ (Fig. 4). When $\gamma_z$ is large [Fig. 4(b)], the cross section decreases faster than the core current decay causing the edge safety factor q ($q \sim a^2/I_p$, $a$

the plasma minor radius) to decrease and thus the poloidal halo current to be larger. As we shall see, reduction of the poloidal halo currents results from keeping q large so that the poloidal halo current is reduced.

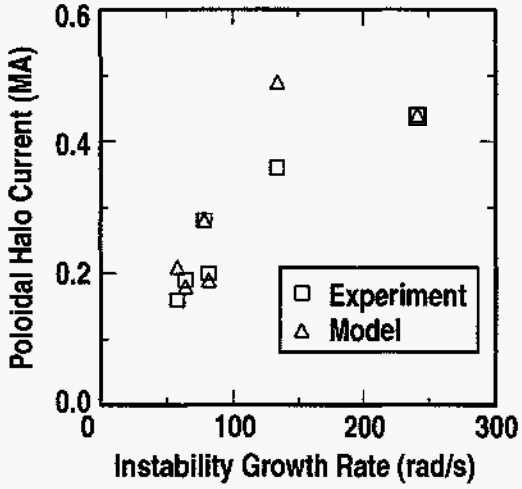


Fig. 3. Halo current versus vertical instability growth rate with fixed current decay rate as experimentally measured and predicted by a model.

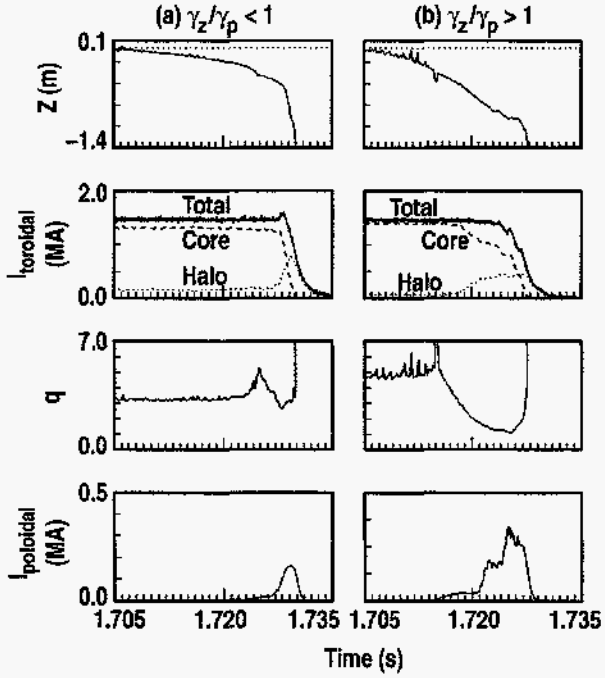


Fig. 4. Comparison of two VDE discharges with a ratio of $\gamma_z/\gamma_p < 1$ [(a) discharge 90204] and $\gamma_z/\gamma_p > 1$ [(b) discharge 90219]. Time evolution of vertical position, total toroidal current, core toroidal current (dashed), halo toroidal current (dotted), edge safety factor q, and total poloidal halo current.

## IV. DISRUPTION MITIGATION RESULTS

The deleterious effects of disruptions, i.e., large halo currents and heat fluxes along with large toroidal asymmetries, require methods to reduce these effects. Experiments on DIII–D that have successfully mitigated disruptions include injection of impurity "killer" pellets of neon and argon and injection of a massive gas puff of helium. Solid pellets of neon and argon with sizes of 1.7, 2.8, and 4 mm were injected with a typical velocity of 500 m/s using a pneumatic injector[19] and penetrated to a normalized radius $\rho = r/a$ (r the minor radius) between $0.2 < \rho < 0.5$. The massive gas puff of helium was accomplished using a fast acting valve developed for the DIII–D pellet injector propellant.[20] The valve mounted 0.5 m from the plasma edge somewhat above the midplane connects a 300 ml reservoir filled to 1000 psi with helium directly to the tokamak. A 10-ms wide gas burst is produced with an average flow rate of $4 \times 10^5$ T-l/s compared to a typical discharge gas fueling rate of ~70 T-l/s; a total of ~3400 T-l of helium is injected.

The pellet injection phenomenology was described previously along with initial mitigation results.[8] Experiments with neon pellets, argon pellets, or massive helium gas puff reduce the force on the vessel by up to 50%.[21] The mitigation of a VDE by injection of a neon impurity pellet is compared in Fig. 1 to a similar discharge without a pellet. The pellet ablates in ~0.7 ms and most of the stored thermal energy is lost during the pellet ablation time. There is a reduction of the poloidal halo current and TPF. Similar behavior is seen in experiments with argon pellets (Fig. 5). Argon, because of its higher Z, is a better radiator and as expected, this results in a

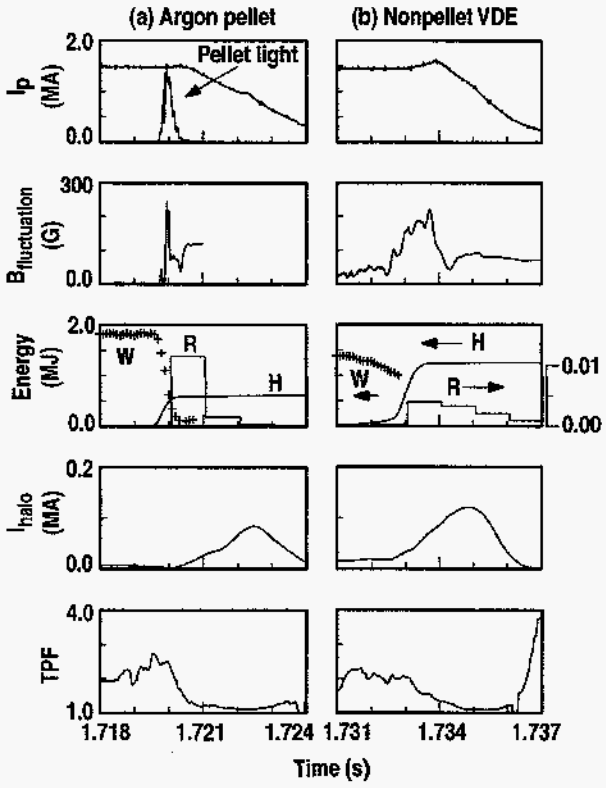


Fig. 5. Comparison of a VDE discharge mitigated with an argon pellet [(a) discharge 90206] versus an unmitigated VDE [(b) discharge 90205]. Time evolution of plasma current, pellet light, poloidal magnetic fluctuation, stored thermal energy (W) calculated from equilibrium fitting code, energy radiated(R) in the time interval represented by each step, the integrated heat to the divertor floor (H), the total poloidal halo current, and the TPF. Note the increased scale for the radiated energy (R) for the unmitigated VDE.

faster cooling with lower halo currents. The MHD for both the pelleted and nonpelleted shot locks and a large n = 1 mode appears ($\delta B/B_T \sim 1\%$). However, the mode growth with the pellet is much more rapid and occurs early in the pellet ablation. Almost all the stored energy is again lost during the pellet ablation time. The pellet reduces the heat flux to the divertor by ~40% and increases the power radiated. The halo current is reduced but for this disruption case, the halo current asymmetry at the time of peak halo current is already relatively low and there is little reduction in the TPF. The experiments with neon and argon pellets have successfully reduced both the halo currents and TPFs and examination of the time history of the signals shows both have been reduced throughout the entire disruption phase.

The mitigation of the axisymmetric poloidal halo current by the pellet is explained by applying the model presented previously to the time evolution of the plasma as shown in Fig. 6 (same neon discharges as in Fig. 1). The pellet injection at 1.718 s occurs before the plasma has moved far off axis, when the cross section is still large, and it triggers the thermal quench within 1 ms followed by the current quench. Although the total current decay with the pellet is slower, the core current decay is faster (1.719 to 1.722 s) than the nonpellet VDE (1.730 to 1.735). The larger minor radius $a$ and the smaller core plasma current both combine to keep the edge safety factor q ($q \sim a^2/I_p$) higher. Thus in the pellet case, although its toroidal halo current is similar to the non-pellet case, the poloidal halo current is reduced $\left(I_h^{pol} = I_h^{tor}/q\right)$.

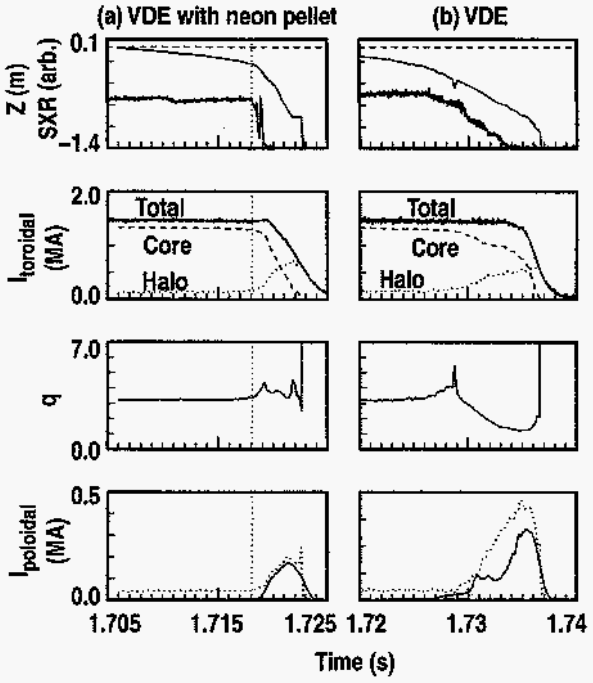


Fig. 6. Comparison of a VDE discharge mitigated with a neon pellet [(a) discharge 88826] versus an unmitigated VDE [(b) discharge 88810]. Time evolution of vertical position, soft x-ray, total toroidal current, core toroidal current (dashed), halo toroidal current (dotted), edge safety factor q, and total poloidal halo current measured (solid) and calculated (dotted). The dotted vertical line in (a) marks the pellet injection time.

The rapid and almost complete loss of the stored thermal energy during the pellet ablation occurs even though the pellet is fully ablated before penetrating to the core of the plasma. For the argon pellet injection (Fig. 5), 0. 6 ms after the pellet injection when the ablation of the pellet is complete, the pellet has only penetrated to $\rho \sim 0.4$ and the stored energy is reduced by 93%.

We hypothesize that this energy quench of the plasma inside $\rho = 0.4$ results from an anomalous rapid transport of the pellet material into the plasma core ahead of the pellet which then causes sufficient impurity radiation to dissipate the plasma's thermal energy.[22] This increased dissipation reduces the heat flux to the divertor. Figure 5 shows a 40% reduction of the integrated heat flux to the divertor.

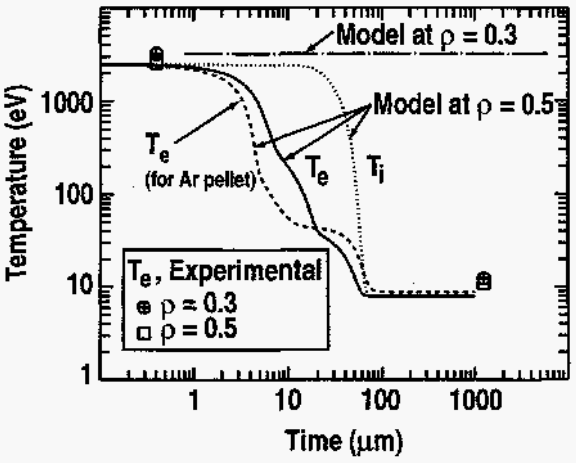


Fig. 7. Time evolution of the electron temperature (solid) and ion temperature (dotted) during a neon pellet ablation as calculated from the KPRAD code at normalized radii of r/a = 0.5 (for discharge 88806) and r/a = 0.3 (dash-dot). Experimental measurements of the electron temperature (from Thomson scattering) before and after the pellet injection at r/a = 0.3 (circle w cross) and r/a = 0.5 (square). Also shown is a KPRAD code calculation of the electron temperature evolution if the pellet material was argon instead of neon (dashed).

The results of the impurity pellet injection mitigation experiments have been modeled by a time-dependent 1–D code (KPRAD) that includes pellet ablation and impurity radiation.[23] The code calculates the radiation and energy balance during the pellet ablation on each flux surface assuming no radial conduction. The time evolution of the electron and ion temperature and the electron density are among the output results of the code. Figure 7 shows the calculated temperature for a neon pellet discharge. Both the ion and electron temperature decrease in less than 0.1 ms, at $\rho = 0.5$. This very rapid cooling is due to the large amount of deposited neon impurity ions (~half the initial electron density). They radiate sufficiently in the lower charge states ($Z_{neon} < +8$) that the electron temperature drops fast enough to halt further ionization of the neon to the less radiative higher charge states.[23] A simulation of the cooling due to this neon pellet with the TSC code,[24] a 2–D time-dependent axisymmetric MHD code, agreed with the KPRAD result when TSC assumed no change in the thermal diffusivity and no radial redistribution of the ablated pellet material. The experimentally measured electron temperatures at $\rho = 0.5$ agree with the KPRAD code prediction, but the code does not predict the measured collapse of the central temperature ($\rho < 0.4$) (Fig. 7).

However, the central temperature collapse can be explained by anomalous penetration of the pellet impurity material into the core. Evidence of this anomalous transport includes an increase in the core density within 1 ms of the pellet injection and spectroscopic measurements of pellet material impurity radiation originating in the core. Both the level of the magnetic fluctuations ($\delta B/B_T \sim 1\%$ in Fig. 5) and their early appearance in the pellet ablation indicate that MHD may be the cause of this anomalous radial transport.[22]

Although the impurity pellet successfully mitigates the halo current, TPF, and heat flux it frequently has the undesirable effect of generating runaway electrons. Runaway electrons are evident in bursts or continuous hard x-rays, nonthermal electron cyclotron emission (ECE), and a plateau in the current decay due to current carried by the runaway electrons (Fig. 8). Signatures from runaway electrons have been observed on all the argon pellet discharges, many of the neon pellet discharges, but none of the nonpellet comparison discharges. The production of runaway electrons cannot be explained by the classical Dreicer runaway mechanism where electrons with energies above a critical energy runaway due to lack of collisions.[25–27] Calculations using the KPRAD code show that the ratio of the critical energy ($E_{crit}$) for runaway generation to the thermal energy ($T_e$) of the bulk plasma drops from ~2000 to ~100 during the pellet injection. This results in an insignificant runaway current (« 1 A/m$^2$). The failure of the classical Dreicer runaway electron generation mechanism was also confirmed in a DINA simulation of a discharge with a clear runaway current plateau (Fig. 8). No runaway current was generated in the DINA simulation which included a runaway current model of "Dreicer" acceleration along with a collisional avalanche mechanism[28–29] term to amplify any Dreicer runaway seed current.

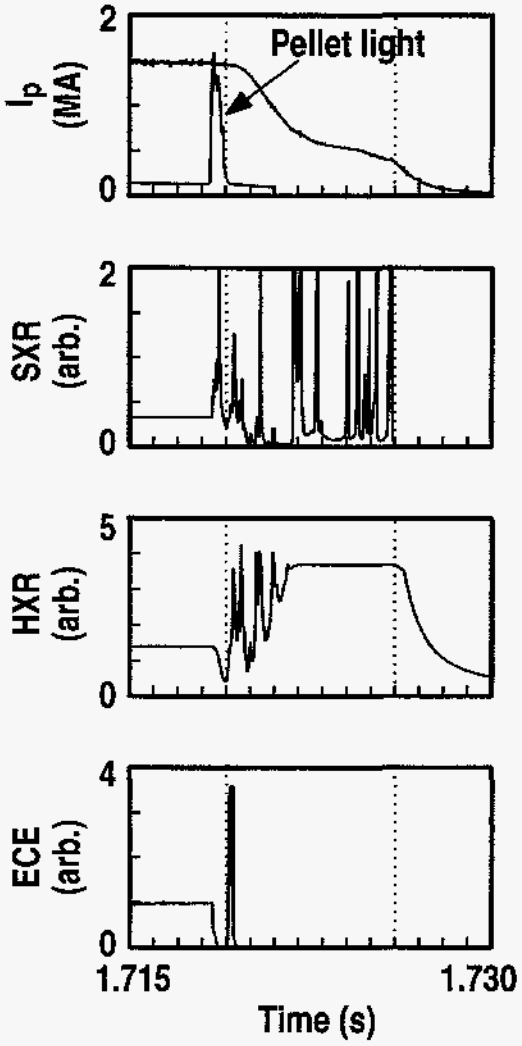


Fig. 8. Time evolution of plasma current, argon pellet ablation light, central soft x-ray radiation, hard x-ray scintillator outside vessel, and RF ECE emission (suffers from density cutoff later in time) for discharge 95180. Evidence of runaway electrons seen after pellet at 1.719 to 1.726 s (times marked by vertical dotted lines).

Two modifications of the standard Dreicer process can provide the observed runaways. Large temperature and pressure gradients across the pellet ablation region can lead to instabilities and, as part of that mixing process, hot electrons from the core can be dumped into the cold, thermally collapsed plasma. These electrons will have a ratio of $E_{crit}/T_e \sim 1$ and will run away. The second modified runaway mechanism is due to the

rapid cooling caused by the pellet. KPRAD calculations of the cooling rates (for the discharge in Fig. 7), as a function of the electron energy, indicate that the cooling time of ~0.03 ms for the bulk electrons is too rapid for the electrons in the tail of the energy distribution function to participate due to the finite collisional coupling times. Test particle calculations with KPRAD show that electrons with energies of 12 times the initial thermal temperature of the bulk plasma or larger will runaway to relativistic energies while electrons with energies of 11 times or less will be cooled.[22–23] A Fokker-Planck code, CQL3D,[30–31] simulation of the discharge in Fig. 7 has also verified this runaway generation mechanism. For the neon pellet, the calculated runaway current density is ~$1.1 \times 10^5$ A/m$^2$ (compared to the initial current density of ~$10^6$ A/m$^2$). This runaway production mechanism is very sensitive to the cooling time of the bulk electrons. Using a KPRAD simulation for argon instead of neon results in a more rapid cooling (Fig. 7) and thus a runaway current density nine times higher (~$9 \times 10^5$ A/m$^2$). This increase in runways with the faster cooling argon impurity pellets explains the experimental observation stated above that runaways are observed in all the argon pellet experiments but only some of the neon experiments. These runaway generation mechanisms provide an initial seed of runaway electrons that can then be amplified by the collisional avalanche mechanism[28–29] to produce the observed runaway current levels (~0.3 MA in Fig. 8).[32]

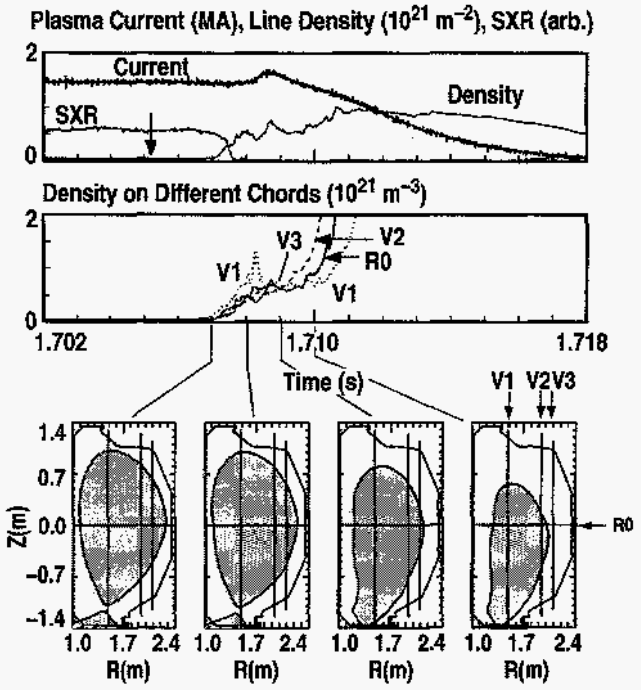


Fig. 9. Massive helium gas puff phenomenology. Plasma current, line density, and average density calculated from the line density along three vertical chords V1, V2, V3 at major radii R = 1.486, 1.942, 2.099 m and 1 horizontal chord at z = 0 m for discharge 96764. Flux plots for four times 1.707 to 1.710 s are also shown with the density chord positions marked. The time the puff valve opens is marked by the arrow.

Results similar to the impurity pellet mitigation, but without the generation of runaway electrons, are obtained in a set of preliminary experiments where a massive puff of helium gas is injected. The phenomenology of the massive gas puff is shown in Fig. 9. In this discharge, there is a large density increase, a thermal quench, and then the beginning of the current quench following ~2, 2.2, and 3 ms, respectively, after the opening of the fast puff valve. The increase in the average density to ~$1 \times 10^{21}$ m$^{-3}$ measured along two vertical chords and one horizontal chord initially track (until 1.709 s) indicating that

the gas has rapidly penetrated to the center and that the density is uniform across the plasma. One vertical chord (V1), passing through the divertor region, is initially larger than the others indicating a large density in the divertor region until the plasma has limited on the floor after which all the chords give the same density (1.7085 to 1.709 s). Only 10% to 20% of the ~$10^{23}$ helium atoms injected are ionized. Later in time, the average density along the chords, which is calculated assuming all the density is in the plasma core, start to diverge due to significant density in the halo region.

The massive helium gas puff mitigates a VDE (Fig. 10) with a reduction of both the halo current and TPF but shows no evidence of runaway electrons [soft x-ray signal (Fig. 9)]. The heat flux in these ohmic discharges is also significantly reduced by the helium puff but has to be inferred since the direct measurement by the IR camera during the helium puff is precluded by line radiation from the helium in the same region of IR used by the camera. The helium puff results in the radiated power increasing by 45% and the fraction coming from the core plasma as opposed to the divertor region increases from 0.64 to 0.82 (Fig. 11). The total energy radiated in the helium puff discharge is equal (within 5%) to the sum of the energy radiated and the energy deposited as heat flux to the divertor in the unmitigated VDE (Fig. 12). Assuming there is no energy conducted to the divertor in the helium puff discharge, the total energy accounting shows the radiation and residual magnetic energy balance to within 5% with the initial thermal and magnetic energy (Fig. 12). Thus since essentially all the energy is appearing as radiation, there is none remaining to be deposited as heat flux on the divertor. Several factors combine to leave unresolved whether the thermal energy is dissipated via radiation or via conduction to the floor. These factors include: a thermal energy in these ohmic discharges that is well below the dominant magnetic

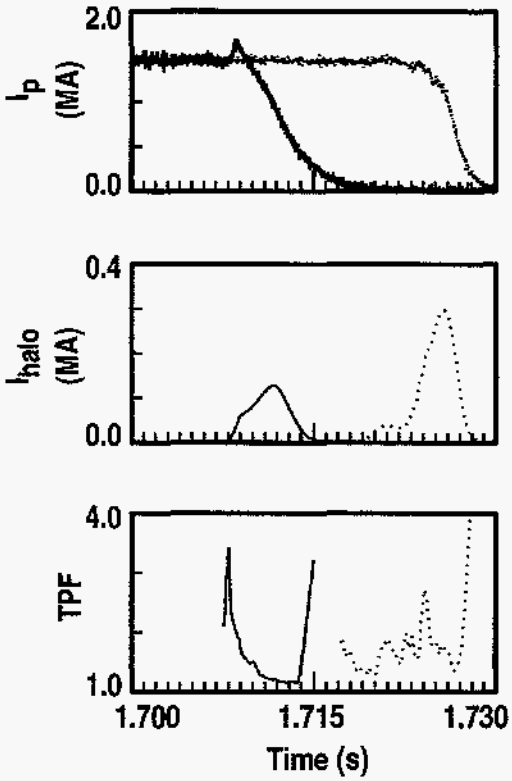


Fig. 10. Comparison of VDE discharge mitigated by a massive helium gas puff (solid, discharge 96764) with an unmitigated VDE (dotted, discharge 96759). Time evolution of plasma current, total poloidal halo current, and TPF of the halo current.

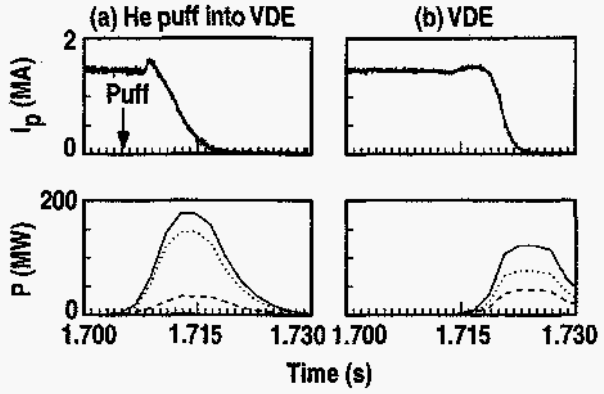


Fig. 11. Comparison of VDE discharge mitigated by a massive helium gas puff [(a) discharge 96762] with an unmitigated VDE [(b) discharge 96757]. Time evolution of the plasma current, total power radiated (solid), core power radiated (dotted), and divertor power radiated (dashed).

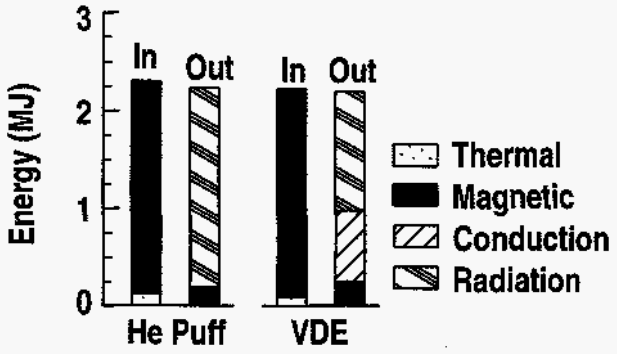


Fig. 12. Energy balance accounting of the energy input to the disruption (IN), which includes initial stored thermal energy and initial magnetic energy (there is no auxiliary heating in this discharge), versus the energy lost during the disruption (OUT) which includes radiation and conduction losses and the residual magnetic energy at the final analysis time. Results for the helium gas puff mitigation and unmitigated VDE discharges in Fig. 11. The conduction for the helium puff is not measured.

energy, the slow time resolution of the bolometer, and the lack of a reliable IR measurement of the conduction to the floor.

A KPRAD simulation provides an understanding for the heat flux mitigation. The temperature dilution from the increasing density, along with energy losses from ionization and radiation decrease the electron temperature to ~6 eV in 2 ms. The plasma becomes dominated by volume recombination (recombination time for $He^{+2}$ ~2 ms for these conditions) and by radiation losses from the hydrogenic ($He^{+1}$) charge state which has a radiative cooling rate of $\sim 3 \times 10^{-35}$ W–m$^3$ at 6 eV. This results in ~30 MW/m$^3$ (or 0.6 GW total) radiated power loss density, in good agreement with experimental radiation measurements (maximum measured 35 MW/m$^3$). The measured UV continuum radiation from the recombination of $He^{+2}$ confirms that the plasma temperature is ~6 eV at the beginning of the current quench in agreement with the modeling. This low electron temperature effectively halts any further ionization of the helium (ionization potential 24.6 eV) and explains why only 10% to 20% of the injected helium is ionized.

Experiments were also performed to see if results similar to the mitigation of disruptions following VDEs occurred for major disruptions. The massive helium gas puff and argon pellet were used to preemptively terminate a discharge near a density limit major disruption (Fig. 13). This figure shows that the results of a helium puff and an argon pellet have a very similar mitigation of the halo current and TPF. The force on the vessel was also reduced in the helium puff case, similar to the pellet mitigation results.

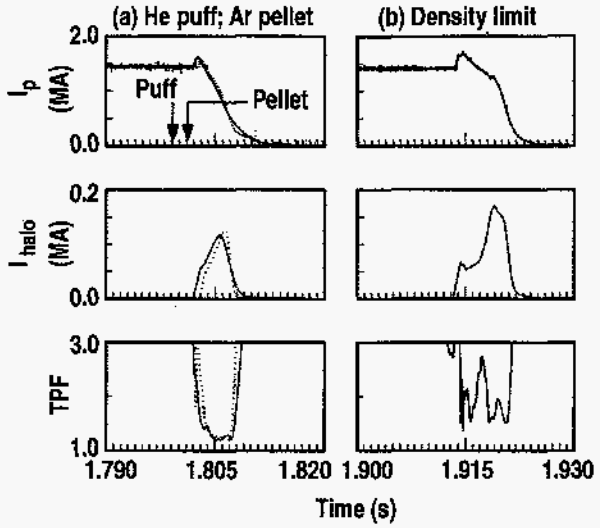


Fig. 13. Comparison of a massive helium gas puff injection [(a) solid, discharge 96767] and an argon pellet injection [(a) dotted, discharge 96768] into repeat of a discharge with a major density limit disruption [(b) discharge 96766]. Time evolution of plasma current, total poloidal halo current, and TPF of the halo current. The injection times of the helium puff and argon pellet are as marked.

The mitigation using the massive helium gas puff injection is encouraging for liquid jet mitigation of disruptions in future large devices such as ITER. In such devices, with large currents (>10 MA) a small initial "seed" of runaway electron current is expected to be amplified by the collisional avalanche mechanism[28–29] to the point that the dominant part of the many mega-ampere plasma current is carried by multi-MeV runaway electrons. To prevent such a generation of runaways, it is necessary to increase the density sufficiently that the increased electric field during the disruption remains below the critical field for the avalanche process.[29,33] In ITER, a 50 to 100 fold density increase would be required and a single pellet or multiple pellets would not be sufficient. Calculations indicate a pulsed liquid jet can meet the mass injection requirement.[33] A fast liquid jet of hydrogen or helium also has a number of advantages for disruption mitigation. During jet injection, there will be isobaric dilution cooling, allowing deep penetration and possibly avoiding MHD driven instabilities due to an unchanged pressure profile. Liquid jets will rapidly cool the plasma (dilution cooling, bremsstrahlung, and recombination radiation cooling) which induces the rapid current decay; thus mitigating the halo current and heat flux load. The high density will also inhibit the formation of runaway electrons.

## V. SUMMARY AND CONCLUSIONS

We have reported on the progress of understanding the mitigation of both major disruptions and vertical displacement events (VDEs) on the DIII–D tokamak. Halo currents with up to 35% of the predisruption plasma current, toroidal peaking factors approaching 3, and heat fluxes of up to 100% of the predisruption thermal energy have been observed in unmitigated discharges. The halo current origin and scaling is well understood and well predicted by a simple analytical model and simulation codes such as DINA and TSC.

DIII–D experiments achieved a similar level of mitigation of both major disruptions and the disruptions following VDEs by preemptively terminating the discharge by injection of impurity pellets of neon and argon and a massive helium gas puff. Injection of impurity pellets into DIII–D plasmas after the initial loss of vertical position have effectively reduced the halo currents, toroidal asymmetry of the halo current, and the heat flux conducted to the divertor that occurred during the disruption at the end of the VDE. Production of runaway electrons, however, have been observed in many of the pellet injection experiments — particularly those using argon. The rapid cooling of the plasma can be explained by a modeling code (KPRAD) and the dissipation of the stored energy inside of the pellet burnup radius can be explained by the observed anomalous rapid transport of the pellet material into the plasma core. The runaway generation can be understood in terms of a modified Dreicer mechanism occurring during the pellet penetration. The first experiments with the injection of a massive amount of helium gas have been explored as an alternative to the impurity pellets in order to eliminate the undesirable runaway electrons. These experiments have shown effective mitigation of the halo currents, halo current asymmetry, and heat flux and have avoided the generation of runaway electrons. Both the impurity pellets and the massive helium gas puff have also been shown to preemptively mitigate a major disruption. Calculations for liquid jet mitigation of future large machines show the promise of the liquid jet idea.

## ACKNOWLEDGMENTS

The authors would like to thank the DIII–D staff for their assistance in the performance of these experiments, Dr. S.C. Jardin for the TSC code simulation, Dr. R.W. Harvey for the CQL3D code simulation, and Dr. R. Khayrutdinov and Dr. R. Lukash for the DINA code simulations.

This work is supported by the U.S. Department of Energy under Contract Nos. DE-AC03-99ER54463, DE-AC05-96OR22464, and DE-AC02-76CH03073, and Grant DE-FG03-95ER54294.

## REFERENCES

[1]J. A. Wesson, R. D. Gill and M. Hugon et al., Nucl. Fusion **29**, 641 (1992).

[2]D. J. Ward and J. A. Wesson, Nucl. Fusion **32**, 1117 (1992).

[3]TFR Group Collaboration, Nucl. Fusion **25**, 919 (1985).

[4]R. Yosino, Y. Neyatani, N. Hosogane, S. W. Wolfe, M. Matsukawa, and H. Ninomiya, Nucl. Fusion **33**, 1599 (1993).

[5]J. C. Wesley and the ITER Joint Central Team, Phys. Plasmas, **4**, 2642 (1997).

[6]J. L. Luxon and L. G. Davis, Fusion Technology **8**, 2A 441 (1985).

[7]T. E. Evans, A. G. Kellman, D. A. Humphreys, M. J. Schaffer, P. L. Taylor, D. G. Whyte, T. C. Jernigan, A. W. Hyatt, and R. L. Lee, J. Nucl. Mater. **241–243**, 606 (1997).

[8]A. G. Kellman, J. W. Cuthbertson, T. E. Evans, D. A. Humphreys, A. W. Hyatt, G. L. Jahns, T. Jernigan, C. J. Lasnier, R. L. Lee, J. A. Leuer, S. Luckhardt, M. J. Schaffer, P. L. Taylor, D. G. Whyte, D. Wroblewski, and J. Zhang, Fusion Energy 1996 (International Atomic Energy Agency, Vienna, 1997) Vol. 1, p.739.

[9]E. J. Strait, L. L. Lao, J. L. Luxon, and E. E. Reis, Nucl. Fusion **31**, 527 (1991).

[10]T. H. Jensen and D. G. Skinner, Phys. Fluids B **2**, 2358 (1990).

[11]R. S. Granetz, I. H. Hutchinson, J. Sorci, J. H. Irby, B. LaBombard, and D. Gwinn, Nucl. Fusion **36**, 545 (1966).

[12]Y. Neyatani, R. Yoshino and T. Ando, Fusion Technology **28**, 1634 (1995).

[13]P. Andrew, P. Miele, P. Noll, R. Pearce, M. Pick, and L. Rossi, Proc. 16th IEEE/NPSS Symposium on Fusion Engineering, Champaign, Illinois, 1995 (Institute of Electrical and Electronics Engineers, Inc., Piscataway, New Jersey, 1996), Vol. 1, 770.

[14]O. Gruber, K. Lackner, G. Pautasso, U. Seidel, and B. Streibl, Plasma Phys. Control. Fusion **35**, B191 (1993).

[15]R. L. Lee, C. J. Lasnier, A. W. Hyatt, A. G. Kellman, P. L. Taylor, Proc. 16th IEEE/NPSS Symposium on Fusion Engineering, Champaign, Illinois, 1995 (Institute of Electrical and Electronics Engineers, Inc., Piscataway, New Jersey, 1996), Vol. 2, 902.

[16]A. W. Hyatt, R. L. Lee, J. W. Cuthbertson, D. A Humphreys, A. G. Kellman, C. J. Lasnier, P. L. Taylor, and the DIII–D Team, Proc. 23rd Euro. Conf. on Controlled Fusion and Plasma Physics, Kiev, Ukraine, 1996, (European Physical Society, 1996) Vol. 20C, 287.

[17]R. Khayrutdinov and R. Lukash, Plasma Phys. Rep. **22**, 91 (1996).

[18]D. A. Humphreys and A. G. Kellman, "Analytic Modeling of Axisymmetric Disruption Halo Currents," submitted to Phys. Plasmas; General Atomics Report GA–A22802 (1998).

[19]L. R. Baylor, B. E. Argo, G. C. Barber, S. K. Combs, M. J. Cole, G. R. Dyer, D. T. Fehling, P. W. Fisher, C. A. Foster, C. R. Foust, M. J. Gouge, T. C. Jernigan, R. A. Langley, S. L. Milora, A. L. Qualls, D. E. Schechter, D. O. Sparks, C. C. Tsai, J. B. Wilgen, and J. H. Whealton, Proc. 15th IEEE/NPSS Symposium on Fusion Engineering, Hyannis, Massachusetts, 1993 (Institute of Electrical and Electronics Engineers, Inc., Piscataway, 1994) Vol. 2, 583.

[20]S. L. Milora, S. K. Combs, and C. R. Foust, Rev. Sci. Instrum. **57**, 2356 (1986).

[21]P. L. Taylor, A. G. Kellman, K. Holtrop, and R. L. Lee, Bull. Amer. Phys. Soc. **37**, 1570 (1992).

[22]D. G. Whyte, T. E. Evans, T. C. Jernigan, A. G. Kellman, R. L. Lee, P. B. Parks, R. E. Stockdale, and P. L. Taylor, "Rapid Inward Impurity Transport During Pellet Injection on the DIII–D Tokamak," to be published in Phys. Rev. Lett.; General Atomics Report GA–A22773 (1998).

[23]D. G. Whyte, T. E. Evans, A. G. Kellman, D. A Humphreys, A. W. Hyatt, T. C. Jernigan, R. L. Lee, S. L. Luckhardt, P. B. Parks, M. J. Schaffer, and P. L. Taylor, Proc. 24th Euro. Conf. on Controlled Fusion and Plasma Physics, Berchtesgaden, Germany, 1997 (European Physical Society, 1997), Vol. 21A, 1137.

[24]R. O. Sayer, Y.-K. M. Peng, S. C. Jardin, A. G. Kellman, and J. C. Wesley, Nucl. Fusion **33**, 969 (1993).

[25]H. Dreicer, Phys. Rev. **117**, 329 (1960).

[26]R. M. Kulsrud, Y. C. Sun, N. K. Windsor and H. A. Fallon, Phys. Rev. Lett. **31**, 690 (1973).

[27]H. Knoepfel and D. A. Spong, Nucl. Fusion **19**, 785 (1979).

[28]R. Jayakumar, H. H. Fleischmann, and S. J. Zweben, Phys. Lett. A **172**, 447 (1993).

[29]M. N. Rosenbluth and S. V. Putinski, Nucl. Fusion **37**, 1355 (1997).

[30]R. W. Harvey and M. G. McCoy, Proc. of IAEA Tech. Comm. Meeting on Advances in Simulation and Modeling of Thermonuclear Plasmas, Montreal, Canada, 1992 (International Atomic Energy Agency, Vienna, 1993) p. 489.

[31]G. D. Kerbel and M. G. McCoy, Phys. Fluids **28**, 3629 (1985).

[32]T. E. Evans, D. G. Whyte, P. L. Taylor, A. G. Kellman, P. B. Parks, D. A. Humphreys, R. W. Harvey, S. C. Luckhardt, T. C. Jernigan, M. J. Schaffer, L. R. Baylor, A. W. Hyatt, R. L. Lee, J. A. Leuer, D. Gray, and J. Zhang, "The Production and Confinement of Runaway Electrons with Impurity 'Killer' Pellets in DIII–D," Proc. 17th Inter. Conf. on Fusion Energy Yokohama, Japan, 1998 (International Atomic Energy Agency, to be published); IAEA-F1-CN-69/EXP3/07; General Atomics Report GA–A22976 (to be printed).

[33]P. B. Parks, M. N. Rosenbluth, S. V. Putvinskij, and T. E. Evans, "High-Velocity Liquid Jet Injection into Tokamak Plasmas for Disruption Mitigation," submitted to Fusion Technology; General Atomics Report GA–A22908 (1998).